International Journal of Plasticity xxx (2016) 1–19

Contents lists available at ScienceDirect

International Journal of Plasticity

journal homepage: www.elsevier.com/locate/ijplas

Transformation stress modeling in new Fe–Mn–Al–Ni shape memory alloy

A. Ojha, H. Sehitoglu*

Department of Mechanical Science and Engineering, University of Illinois at Urbana-Champaign, 1206 W. Green Street, Urbana, IL 61801, USA

ARTICLE INFO

Article history:
Received 13 June 2016
Received in revised form 12 August 2016
Available online 31 August 2016

Keywords:
A. Phase transformation
A. Twinning
A. Dislocations
B. Constitutive behavior
FeMnAlNi shape memory alloy

ABSTRACT

We investigate the bcc-fcc transformation in the new shape memory alloy FeMnAlNi utilizing density functional theory calculations for double shear. We formulate an energy expression to derive the fcc martensite formation stress, incorporating the transformation shear energy and the elastic interactions of the dislocations. The critical bcc-fcc transformation stress was determined as 191 MPa, which is close to the experiments. Concurrently, we also establish the fcc twinning and slip stresses as 201 MPa and 335 MPa respectively. The higher slip resistance ensures recoverability of the transformation. We observe that the Bogers-Burgers double shear mechanism proceeds with a much lower energy barrier and is favored over the 'classical' Bain deformation. Overall, the parameters obtained from DFT calculations are devoid of any empiricism and the prediction of these critical stresses permit the design of new iron based SMAs.

1. Introduction

1.1. Fundamentals of shape memory- iron based SMAs

The field of SMAs has been dominated by NiTi alloys (Duerig et al., 1990; Lagoudas, 2008; Gall et al., 1999; Otsuka and Wayman, 1999; Sehitoglu et al., 2000; Miyazaki and Otsuka, 1989). The iron based alloys have tremendous potential but not well studied. The iron based alloys do not exhibit crystallographic order, have large tetragonality ratios, and finite volumetric strains. All these factors typically curtail shape memory behavior. Low transformation temperatures and large hysteresis in Fe-based SMAs have been reported (Kokorin et al., 1993; Koval et al., 1979; Ando et al., 2009; Sehitoglu et al., 2001, 2002; Maki et al., 1989) which have limited their widespread use. The early work has been conducted on FeNiCoTi based alloys (Sehitoglu et al., 2001, 2002) and reviews and books cover iron based shape memory alloys (Miyazaki and Otsuka, 1989; Otsuka and Wayman, 1999) but to a much less extent than NiTi alloys. The FeNiCoTi has a very wide hysteresis that precludes superelasticity. Major success is now within reach with new class of FeMnAlNi alloys (Omori et al., 2011; Tseng et al., 2015a, 2016) that exhibit superior superelastic properties and removes most of the limitations above. They exhibit transformation strains exceeding 8%, and undergo superelasticity response at room temperature with low stress hysteresis. The iron based alloys are purported to have low slip resistance. As we will show in this study FeMnAlNi exhibits excellent slip resistance.

* Corresponding author.
E-mail address: huseyin@illinois.edu (H. Sehitoglu).

http://dx.doi.org/10.1016/j.ijplas.2016.08.003
0749-6419/

Please cite this article in press as: Ojha, A., Sehitoglu, H., Transformation stress modeling in new Fe–Mn–Al–Ni shape memory alloy, International Journal of Plasticity (2016), http://dx.doi.org/10.1016/j.ijplas.2016.08.003

One of the characteristics of FeMnAlNi alloy is that the stress required to induce martensitic transformation has a low temperature dependence over a broad range, −196 to 240 °C. For example, the Clausius- Clapeyron slope ($d\sigma/dT$) in FeMnAlNi was reported as 0.53 MPa/°C (Tseng et al., 2015b), which is much lower than other SMAs such as NiTi (6–8 MPa/°C (Sehitoglu et al., 2000) in NiTi). The low slope combined with high slip resistance in FeMnAlNi ensures that transformation can occur without reaching slip stress at macroscale.

The FeMnAlNi alloy exhibits superelastic behavior via reversible transformation from body centered cubic (bcc) austenite to face centered cubic (fcc) martensite upon loading and the reversal of phase upon unloading. Although the rearrangements of atoms for fcc and bcc lattices (Bogers and Burgers, 1964; Burgers, 1934; Olson and Cohen, 1976a, b) are known, no studies have focused on a rigorous derivation of transformation stresses. In addition to transformation stress, we established critical stress required for nucleation of the twins in fcc lattice and the stress levels to reach slip mediated deformation in fcc and bcc lattices. To achieve superior shape memory, the slip resistance needs to be rather high to minimize activation and multiplication of dislocations at transformation interfaces.

Considerable efforts have been made to devise continuum formulations to predict the response of shape memory alloys (Gall and Sehitoglu, 1999; Gall et al., 1999; Lagoudas, 2008; Lagoudas and Entchev, 2004; Moumni et al., 2008; Patoor et al., 1995; Qidwai and Lagoudas, 2000; Sedlak et al., 2012; Yu et al., 2014; Zaki and Moumni, 2007). One set of works – the continuum state variable models are based on the yield functions associated with martensitic transformation, the martensite volume fraction evolution and the associated flow rules to model the stress-strain response. Qidwai and Lagoudas (2000) proposed a general form of the yield function to capture tension-compression asymmetry in polycrystalline NiTi. The proposed yield function for transformation depends on the experimentally deduced critical transformation stress. The critical transformation stress and the twinning stress, as material constants, also appear in the martensitic transformation criteria in other formulations (Thamburaja and Anand, 2001, 2002), which we theoretically determine in the present case for FeMnAlNi shape memory alloy.

Further modeling efforts (Lagoudas and Entchev, 2004; Yu et al., 2014; Hamilton et al., 2004) were undertaken to account for the plastic strain accumulation, and multi-dimensional empirically based formulations were proposed that simultaneously captured the evolution of transformation strains and plastic strains with cycling. The plastic strain accumulation is due to the nucleation of slip dislocations at austenite/martensite interface where stresses and strains are rather high, and is governed by the CRSS for slip. The modeling approaches to capture the recoverable strains due to reorientation of martensites have also been proposed (Moumni et al., 2008; Sedlak et al., 2012; Yu et al., 2015; Zaki and Moumni, 2007). These models couple transformation and martensite reorientation in shape memory alloys by incorporating the dissipation potentials in their formulation with an aim to accurately capture shape memory effect, pseudoelasticity, twinning and detwinning of martensite. The derived yield functions and the flow rules for the martensite reorientation in these models are governed by the twinning stress as it relates to the nucleation and motion of twin interfaces, while the transformation yield function is dictated by the critical transformation stress. The theoretical determination of these three crucial modeling parameters - the critical phase transformation, twinning and slip stresses are considered in the present study for FeMnAlNi alloy.

The other set of works- (ii) the micromechanical models are built upon the critical transformation stress as the driving force for phase transformation (Gall and Sehitoglu, 1999; Gall et al., 1999; Patoor et al., 1995). These models incorporate microstructurally informed quantities such as transformation shear magnitudes and consider multiple variant–variant interactions to model the continuum shape memory response. For example, the micromechanical model of Gall and Sehitoglu (1999) incorporated single-crystal constitutive equations and experimentally measured polycrystalline texture into self-consistent formulations to study tension/compression asymmetry in polycrystalline NiTi alloys. The phase transformation criterion in these formulations is based on the critical stress level for martensitic transformation, which is obtained experimentally. One of the key steps to advance these formulations further is to develop a model where the driving forces governing martensitic transformation such as transformation and twinning stresses can be precisely determined with no empiricism. These parameters can in turn provide a key input to these phenomenological models. The community has reached a level of achievement with these mesoscale formulations, and more recently it is recognized that the synergy between the transformation and slip appears to play a role in polycrystalline response (Paranjape et al., 2015; Richards et al., 2013). It is imperative that further advances in the existing transformation mechanisms can be made with a precise determination of the transformation, twinning, and slip stress magnitudes respectively, and is the topic of the present study.

It is difficult to extract the slip, twinning and transformation events precisely from experiments as they could be activated simultaneously or require in-situ high resolution image correlation techniques (Efstathiou et al., 2008; Ezaz et al., 2012). At this time, these quantities are inferred from experiments on a case by case basis. In this study, we believe that a significant benefit could be realized if the transformation stress, slip stress (or CRSS) and twinning stresses are determined theoretically based on atomistic considerations. This has not been a simple task especially for the case of transformation stress where the martensite nucleation formation involves complex atomic level displacements on different planes and shuffles. For stress-induced transformation, the derivation of transformation stress is of paramount importance, but it has not been achieved in early work because of the complexity and is the focus of this study. For example, if shape memory response below martensite finish temperature (M_f) is of interest, the twinning stress is governing. The twinning (and detwinning) behavior dictates the maximum transformation strains achieved in shape memory alloys (Sehitoglu et al., 2003). If the twinning (hence detwinning stress) is not much higher than the transformation stress then the martensite can reach higher transformation strains especially in tension. The calculation of twinning stress can also be

Please cite this article in press as: Ojha, A., Sehitoglu, H., Transformation stress modeling in new Fe–Mn–Al–Ni shape memory alloy, International Journal of Plasticity (2016), http://dx.doi.org/10.1016/j.ijplas.2016.08.003

crystallographically complex (Ezaz et al., 2011) due to the low symmetry planes and multicomponent elements in shape memory alloys. Finally, to study accumulation of permanent strains and to better understand the polycrystalline response with plasticity and transformation governed grains, the determination of slip stress is of paramount importance. The determination of slip stress is simpler (Ezaz et al., 2013) compared to transformation and twinning stress determination. The current work provides a novel approach to derive these important parameters from a combined atomistic/continuum treatment.

1.2. Brief review of FeMnAlNi SMA behavior

In Fig. 1, we show the superelastic response of <123> oriented FeMnAlNi single crystal deformed in tension at room temperature (Tseng et al., 2016). It is important to note that strains near 7% were recovered upon unloading. Several factors such as composition of alloying elements, crystal orientation, and aging could affect the results. In Fig. 1, we also show the parameters of interest, the critical transformation stress ($\tau_{\text{crit}}^{\text{trans}}$), at which the parent bcc austenite transforms into the fcc martensite, the twinning stress, the slip stress for fcc martensite and the slip stress for bcc austenite.

Recent experimental results (Tseng et al., 2015b, 2016; Vollmer et al., 2015) have found high recovery strains of approximately 8% in $Fe_{43.5}Mn_{34}Al_{15}Ni_{7.5}$ upon tensile deformation. The theoretical strain is higher for the case of [100] tension (26.5%) compared to the [123] orientation (14%) as we discuss later, however the ductility could be limiting in [100] crystals. These theoretical transformation strains are rather high and can be beneficial along with the higher stiffness of the iron based alloys compared to NiTi. The slip at interfaces is known to curtail recoverability not only in Fe based SMAs but in other SMAs as well (Ibarra et al., 2007), so studies that calculate the slip stress and potentially improve slip resistance could be substantially useful for advancements of new SMAs. The works of Sehitoglu et al. (2001, 2002) have also highlighted the role of planar dislocations in curtailing reversibility both in single and polycrystalline FeNiCoTi SMAs. The importance of such dislocations at the austenite/martensite interface during phase transformation has been discussed in detail in other shape memory alloys as well (Gall et al., 1998; Norfleet et al., 2009; Simon et al., 2010).

1.3. Bain transformation and Bogers-Burgers double shear

In the present work, we specially look into two widely accepted transformation mechanisms- (i) the Bain distortion and (ii) the Bogers Burgers double shear mechanism to address the critical bcc-fcc transformation stress in FeMnAlNi alloy (Bogers and Burgers, 1964). In the case of (i) Bain deformation, an fcc crystal is formed from the bcc crystal by elongation on the $<001>_{bcc}$ axis and compression along $<010>_{bcc}$ axes. Note that the c/a ratio for bcc crystal is equal to 1 while that of the fcc crystal is equal to $\sqrt{2}$, as shown in Fig. 2. In the case of Bogers Burgers mechanism (ii), two successive shears are responsible for the transformation of the bcc to fcc crystal. The first shear occurs on the $\{110\}<110>_{bcc}$ system and the second shear acts on $\{111\}_{fcc}$ plane along the $<112>_{fcc}$ direction. We note that the energy profile associated with these two transformation paths to be different. Such an understanding of the energy profiles has not been developed in the literature, which we undertake in the present study. Then, our main contribution is to devise an atomistic-continuum model to capture the transformation stress with no a priori assumptions.

In the present work, we find the Borgers-Burgers mechanism to be more energetically favorable compared to the Bain case based on DFT calculations. Consequently, we develop a modified Peierls Nabarro (PN) formalism (based on early works

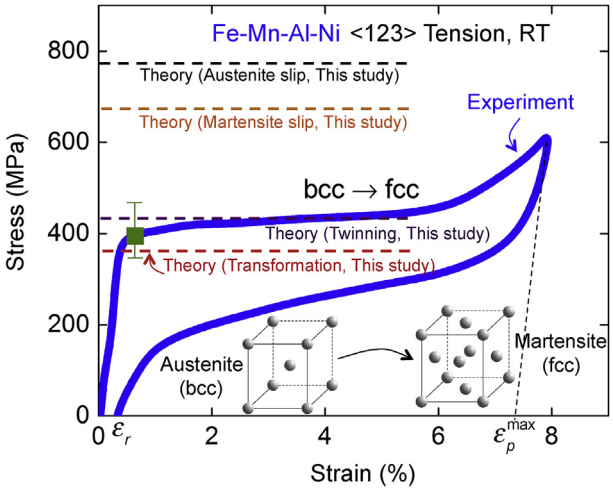

Fig. 1. Superelastic response of <123> oriented FeMnAlNi single crystal subjected to tension at room temperature. Experimental data are taken from Tseng et al. (2016), while theoretical values are obtained from current study.

Please cite this article in press as: Ojha, A., Sehitoglu, H., Transformation stress modeling in new Fe–Mn–Al–Ni shape memory alloy, International Journal of Plasticity (2016), http://dx.doi.org/10.1016/j.ijplas.2016.08.003

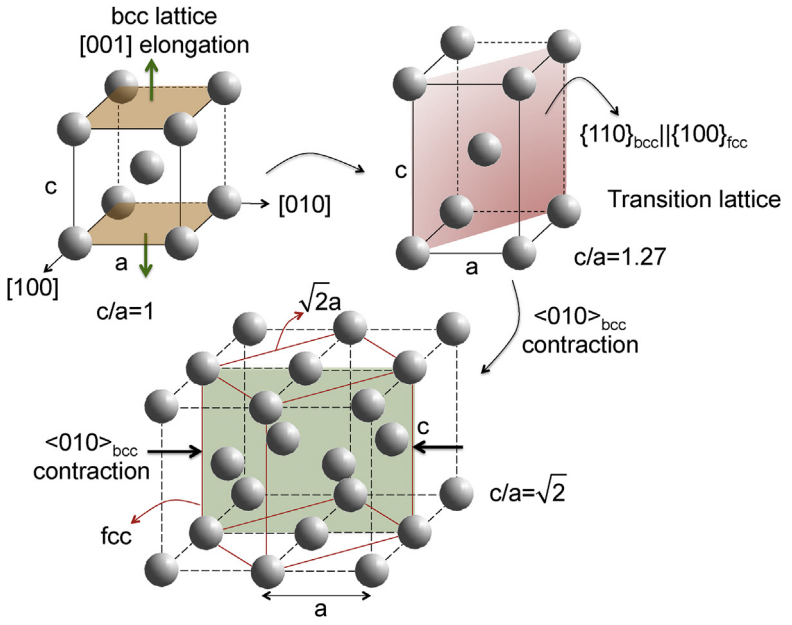

Fig. 2. The bcc-fcc transformation via Bain distortion. The <001> axis of the bcc crystal undergoes elongation while the $<010>_{bcc}$ axes undergo contraction to form the fcc crystal.

on PN (Carrez et al., 2007; Joos and Duesbery, 1997; Joós et al., 1994; Lu et al., 2000; Peierls, 1940)) and forward a theoretical model for bcc-fcc transformation stress. Once the transformation occurs, the martensite deforms by motion of twin interfaces. Concurrently, we predict the twinning stress in fcc martensite by incorporating the Generalized Planar Fault Energy (GPFE) (Wang and Sehitoglu, 2013) with the elastic interactions of the dislocations. During the calculation of the GPFE, the positions of the dislocations on the fault are taken into account, as well as the role of solute atoms close to the fault which can significantly reduce the stacking fault energy (Finkenstadt and Johnson, 2006; Suzuki, 1962). Since FeMnAlNi is a multicomponent alloy, it is important to investigate the effect of each element on the stacking fault energy on an iterative basis. A number of atoms of each element are placed at different positions away from the fault, and the corresponding energies are noted. We repeat this procedure for each element, and the GPFE with the minimum value of stacking fault energy is used to obtain the critical twinning stress in our calculations. The details will be discussed later.

In the current study, it is worth emphasizing that the theoretical model for transformation is built upon heterogeneous dislocation-based transformation mechanism with shear glide on S/3 and S/2 systems (glide every third and second plane respectively). The heterogeneous dislocation based transformation mechanism has been proposed (Olson and Cohen, 1976a, b) for a double shear associated with the fcc-bcc transformation. The impetus in this work is to consider the bcc-fcc transformation, establish the energy barriers, and incorporate the strain energy associated with the participating dislocations. The transformation stress is then derived theoretically which is in excellent agreement with experiments.

According to the phenomenological theory of martensitic transformation (Ahmed and Rack, 1996; Bowles and Mackenzie, 1954; Christian, 2002; Mackenzie and Bowles, 1954; Nishiyama, 2012; Porter et al., 2009; Wayman, 1994), there exists an undistorted and unrotated interface between the parent austenite and the transformed martensite and the deformation is valid invariant plane strain (IPS). The IPS refers to the homogeneous distortion in which the displacement of atom is proportional to the distance of atom from the habit plane. In this context, the Bain deformation does not fulfill the requirements for an undistorted plane, and therefore additional shears in the form of transformation twinning or slip, called lattice invariant shear (LIS) is required. The twin variants in the martensite exhibit the strain tensors illustrated in Fig. 3. The Bain deformation within multivariant martensite twins reduces the strain energy of the transformed martensite.

The importance of the preexisting stacking faults associated with the partial dislocations has been recognized as the precursor to fcc-bcc martensitic transformation, and is the basis for the heterogeneous transformation mechanism (Olson and Cohen, 1976a, b). Note that the present analysis, however holds for the reverse bcc-fcc transformation mechanism. Nonetheless, it is important to point out the relevance of the dislocations partaking in the fcc-bcc transformation to understand the reverse bcc-fcc transformation mechanism. For the case of fcc-bcc transformation mechanism, specially, the intersection of the ε-phase (intermediate hcp phase) with each other or with the twin and grain boundaries are observed to induce body centered cubic martensitic phases.

Bogers-Burgers initially proposed a hard sphere model for the fcc-bcc martensitic transformation via double shear mechanism (Bogers and Burgers, 1964). The Bogers-Burgers mechanism for the fcc→bcc transformation involve two successive or simultaneous homogeneous shears: a/18[112] on every $(11\bar{1})_{fcc}$ plane, and then a shear of a/12[211] on every

Please cite this article in press as: Ojha, A., Sehitoglu, H., Transformation stress modeling in new Fe–Mn–Al–Ni shape memory alloy, International Journal of Plasticity (2016), http://dx.doi.org/10.1016/j.ijplas.2016.08.003

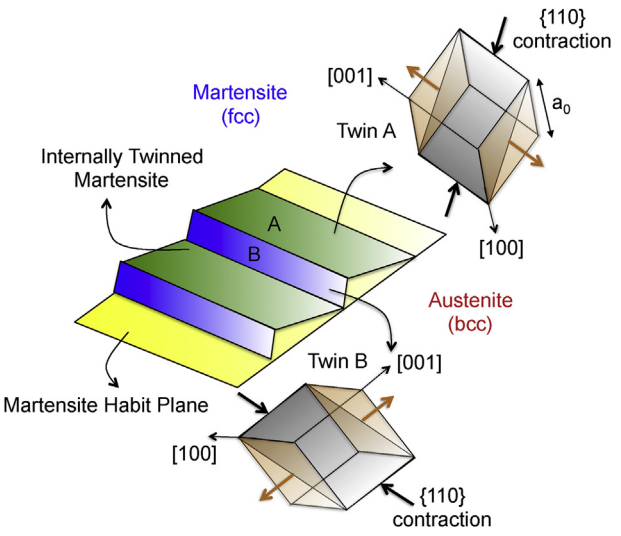

Fig. 3. The additional strains from Bain distortion during phase transformation must be negated via internally twinned martensites which undergo contraction along different axes.

$(\overline{1}\overline{1}1)_{fcc}$ plane, where 'a' is the lattice constant of the fcc phase. These two shears when applied to an fcc crystal will form the correct stacking sequence of the bcc crystal. Note that the first shear (referred to as T/3) is one-third of the twinning partial, and the second shear (T/2) is one-half of the twinning partial in fcc crystal. It is important to note that these shears are applicable for fcc-bcc transformation. However, the bcc-fcc transformation can be accomplished in a similar manner by implementing the Bogers-Burgers mechanism in reverse. This will be discussed next.

The works of Olson and Cohen (1976a, b) further rationalized the homogeneous Bogers-Burgers double shear mechanism by introducing Shockley partials, and their interaction. The first shear (T/3) as suggested by Bogers Burgers mechanism is accomplished by spreading a group of a/6<211> dislocations on every third $(\overline{1}11)_{fcc}$ plane while the second shear (T/2) is accomplished by spreading a group of a/6$[21\overline{1}]$ dislocations on every second {112} plane. The intersection of these two array of dislocations creates a region containing the bcc crystal. Recently, the existence of such dislocation based transformation as proposed by Olson and Cohen has been validated experimentally with the aid of high-resolution TEM measurements (Yang et al., 2014), and molecular dynamics simulations (Sinclair and Hoagland, 2008). However, no prediction of stress for the martensite nucleus has been obtained in previous work.

In this study, on the other hand, we consider bcc-fcc transformation. The bcc-fcc transformation can be obtained first by passing the a_0/8<110> dislocations on every second {110} plane in equal and opposite <110> directions (referred to as collinear shear, S/2 on *B*-plane atoms) as shown in Fig. 4(a). This process transforms the $\{110\}_{bcc}$ plane into the $\{111\}_{fcc}$ plane resulting in an intermediate fcc structure with correct $\{111\}_{fcc}$ stacking sequence. Secondly, as depicted pictorially in Fig. 4(a), consecutive shears on every third $\{111\}_{fcc}$ plane (referred to as S/3 shear on *A*-plane atoms) achieved by passing a/6<112> dislocations result in the final fcc product with correct angle (60°) between the <111> directions. Equivalently, the S/2 shear can also be accomplished by passing two a_0/8<110> dislocations on every second {110} plane ($2b_p$, $4b_p$ and so on) to form an intermediate fcc structure as shown in Fig. 4(b). The faulted structure formed due to the passage of a/6<112> dislocations (b_p, $2b_p$ and so on) on {111} planes in an fcc crystal is shown in Fig. 4(c). Hereafter, the shear on the {110}<110> system will be referred to as *S*/2 shear and the shear on the {111}<112> system as *S*/3 shear.

1.4. The current work, the bcc to fcc transformation

We consider that the double shear mechanism for bcc to fcc transformation is accomplished by the motion of two sets of dislocations, a_0/8<110> and a/6<112>, on different planes in a bcc crystal, the intersection of which forms the fcc crystal, as shown in Fig. 5.

Since the lattice constants are important parameters in the PN formalism based transformation model, an accurate determination of these quantities is important. Therefore, we undertake lattice constant determination of both phases using the DFT calculations (discussed next). In the present paper, we also calculate the maximum transformation strains associated with the bcc-fcc transformation using the lattice deformation theory (LDT) (Bhattacharya, 2003; Saburi and Nenno, 1981). The LDT assumes that a parent bcc crystal transforms into an fcc crystal via the change in lattice constants.

We organized the paper as follows. In Section 2, we discuss our theoretical approach of atomistic calculations and the methodology to obtain the lattice parameters. In Sections 3 and 3.1, we discuss the model development of bcc-fcc transformation. Similarly, in Section 3.2, we discuss the twinning stress formulation and the associated GPFE. In Sections 4 and 5, we provide discussion of the results and the summary respectively.

Please cite this article in press as: Ojha, A., Sehitoglu, H., Transformation stress modeling in new Fe–Mn–Al–Ni shape memory alloy, International Journal of Plasticity (2016), http://dx.doi.org/10.1016/j.ijplas.2016.08.003

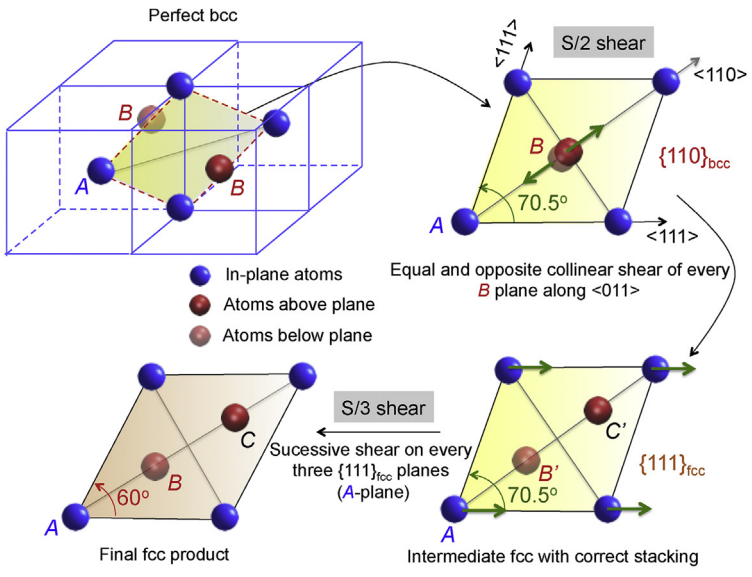

(a)

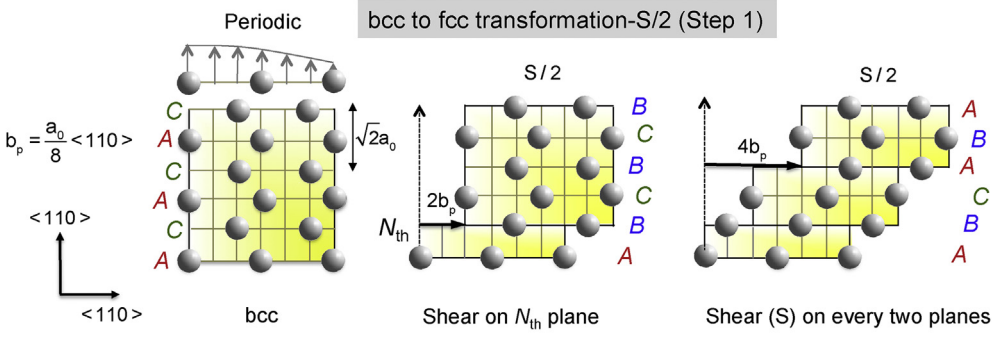

(b)

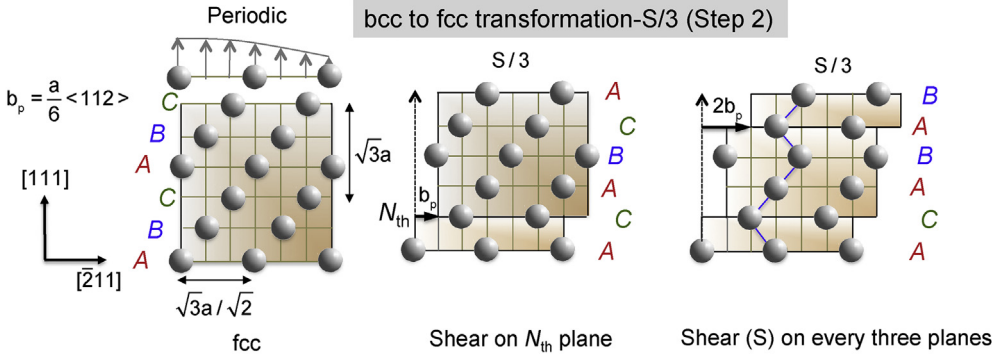

(c)

Fig. 4. Schematics of (a) bcc-fcc transformation via double shear mechanism (S/2 and S/3 shears) (b) the faulted bcc structure subjected to S/2 shear on {110}<110> system and (c) the faulted fcc structure formed by {111}<112> shear considered in the present analysis.

Please cite this article in press as: Ojha, A., Sehitoglu, H., Transformation stress modeling in new Fe–Mn–Al–Ni shape memory alloy, International Journal of Plasticity (2016), http://dx.doi.org/10.1016/j.ijplas.2016.08.003

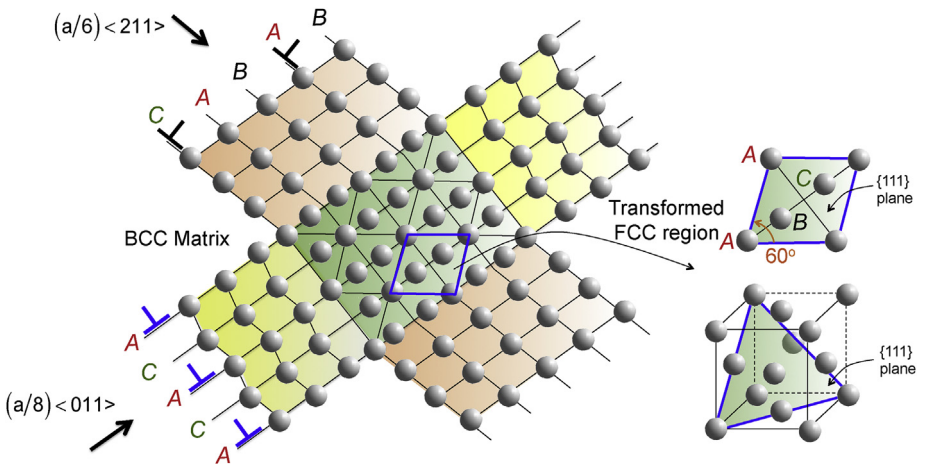

Fig. 5. Heterogeneous dislocation based bcc-fcc transformation mechanism as considered in this study.

2. Simulation methods and lattice constants

We used the first-principles DFT calculations to compute the total structural energy of the crystal. The DFT was implemented using the Vienna ab initio Simulations Package (VASP) with the projector augmented wave (PAW) method and the generalized gradient approximation (GGA) (Kresse and Furthmüller, 1996; Kresse and Hafner, 1993). A $2 \times 7 \times 2$ supercell consisting of 112 atoms was used for simulating a disordered fcc crystal, and the Fe,Mn,Al,Ni atoms were positioned randomly within the supercell depending on the composition (Fe-34 at.%Mn-15 at.%Al-7.1 at.%Ni) and the fcc crystal coordinates. Hereafter, the composition Fe-34 at.%Mn-15 at.%Al-7.1 at.%Ni is referred to as FeMnAlNi. The Monkhorst Pack *k*-point meshes for the Brillouion-zone integration used was $12 \times 5 \times 12$, and the convergence of the structural energy was verified. Note that the *k*-points chosen are inversely proportional to the ratio of the lattice vectors of the supercell for uniform sampling of the *k*-space. Similar procedure was followed for calculating the energy associated with the bcc-fcc transformation path. Ionic relaxation was performed by a conjugate gradient algorithm. The energy cut-off of 360 eV was used for the plane-wave basis set. The total energy was converged to less than 10^{-5} eV per atom.

2.1. Lattice constant calculations

Fig. 6(a) and (b) show the total structural energy variation as a function of the lattice parameters of the bcc and fcc unit cells respectively for Fe–Mn–Al–Ni. The equilibrium lattice constant is taken as the one that corresponds to the minimum structural energy. From our calculations, the lattice constant of bcc crystal is determined as 2.88 Å and that of the fcc lattice is 3.65 Å. The experimentally measured lattice constants are 2.903 Å and 3.672 Å for bcc and fcc crystals respectively (Omori et al., 2011). Note that the theoretical lattice constant values are in close agreement with the experimental values (see Table 1). Hereafter, we refer 'a_o' as the lattice constant of the bcc unit cell, and 'a' that of the fcc unit cell.

3. Energetics of the Bain and Bogers-Burgers shear mechanism

Among the bcc-fcc transformation mechanisms (Bogers and Burgers, 1964; Olson and Cohen, 1976a, b) discussed in the literature, the Bain distortion is considered to be the simplest homogeneous martensite transformation mechanism. As noted earlier in Fig. 2, the bcc structure has a c/a ratio equal to 1. If the bcc lattice is elongated along the <100> axis and contracted along both <010> axes such that the c/a ratio changes to $\sqrt{2}$, the lattice transforms to an fcc structure. The {110} plane of the bcc lattice corresponds to the {111} face of the fcc lattice. In summary, the following lattice correspondence exists between the bcc and the fcc crystal:

$$\left[01\bar{1}\right]_{bcc} \| [100]_{fcc}; [011]_{bcc} \| [010]_{fcc}; [001]_{bcc} \| [001]_{fcc} \tag{1}$$

Fig. 7 shows the energy landscape of the bcc-fcc transformation via the Bain path. Note that no shuffle is required for this transformation unlike the bcc-hcp transformation. The transformation proceeds through an energy barrier ($\gamma^{u}_{Bain} = 594 mJm^{-2}$) corresponding to an unstable configuration. This barrier must be overcome by the applied stress or temperature to attain the product fcc phase. Overall, the transformation mechanism via Bain distortion may be accomplished by internal stresses inherently present in the crystal in the form of defects, precipitates or second phase particles.

Please cite this article in press as: Ojha, A., Sehitoglu, H., Transformation stress modeling in new Fe–Mn–Al–Ni shape memory alloy, International Journal of Plasticity (2016), http://dx.doi.org/10.1016/j.ijplas.2016.08.003

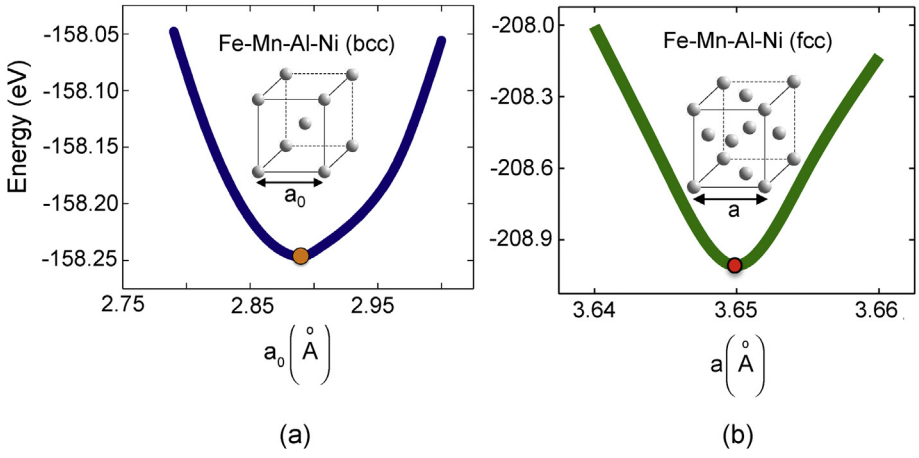

Fig. 6. Structural energy variation with lattice parameters in (a) austenite bcc crystal (b) martensite fcc crystal.

As noted earlier, the bcc-fcc lattice transformation can be obtained by implementing the fcc-bcc transformation in reverse with the aid of dislocations. Consider the following dissociation of an $a_o/2<111>$ dislocation in the bcc crystal:

$$\frac{a_o}{2}\left[1\bar{1}1\right] \rightarrow \frac{a_o}{8}\left[0\bar{1}1\right] + \frac{a_o}{8}\left[1\bar{1}1\right] + \frac{a_o}{4}\left[2\bar{1}1\right] \tag{2}$$

The first shear, $S/2$ of the Bogers Burgers bcc-fcc mechanism can be achieved by passing $a_o/8<110>$ dislocations on every second {110} plane in alternate and opposite directions. This process transforms the $\{110\}_{bcc}$ plane to the $\{111\}_{fcc}$ plane. Note that $a_o/8<110>$ dislocation is equivalent to $a/12<112>$ dislocation in an fcc crystal required to induce the second shear (T/2) of the Bogers Burgers fcc-bcc transformation mechanism. The second inverse Bogers Burgers shear, $S/3$ for the bcc-fcc transformation is accomplished by a shear on each of the transformed $\{111\}_{fcc}$ planes by $a/6<112>$ dislocation, thus leading to an fcc crystal (Fig. 4(a)). During these consecutive or simultaneous shearing processes, the dislocations in the bcc crystal have to overcome an energy barrier to transform to an fcc crystal. In the present case, we calculated the energy barrier profile associated with this transformation in the form a fault energy curve ($\gamma-$curve). For $\gamma-$curve calculation associated with the dislocation based double shear mechanism, the crystal axes are oriented along the $x = [\bar{1}10]$, y=[110] and $z = [00\bar{1}]$ directions. The supercell consists of 13 {110} layers so that the periodic interfaces do not interact. Every second $\{110\}_{bcc}$ planes are sheared consecutively followed by the shear on each of the $\{111\}_{fcc}$ planes to form an fcc crystal. Concurrently, the atoms are allowed to relax during the crystal minimization process. The energy per unit area of the sheared structures with respect to the undeformed crystal were obtained as follows:

$$\gamma = \frac{E_s - E_o}{A_{\{110\}}} \tag{3}$$

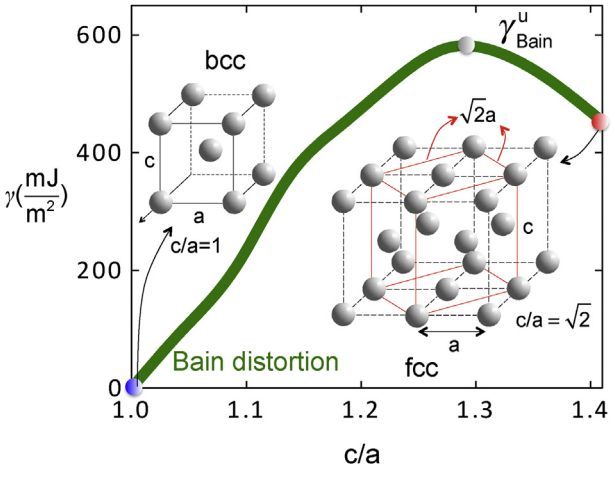

Fig. 7. Energy barrier profile (γ-curve) associated with bcc-fcc transformation via Bain distortion in FeMnAlNi alloy.

Please cite this article in press as: Ojha, A., Sehitoglu, H., Transformation stress modeling in new Fe–Mn–Al–Ni shape memory alloy, International Journal of Plasticity (2016), http://dx.doi.org/10.1016/j.ijplas.2016.08.003

where $A_{\{110\}}$ is the area of the {110} plane (or y-plane) of the simulation box, E_s is the energy of the sheared crystal and E_0 that of the perfect undeformed crystal. We followed similar procedure to obtain the γ-curve for the $S/3$ shearing. The results of the γ-curve associated with the heterogeneous martensitic transformation mechanism for FeMnAlNi alloy is shown in Fig. 9. It should be noted that the maximum energy barrier for the case of Bain deformation is higher than that of the Bogers Burgers mechanism by approximately 192 mJm^{-2}. The maximum unstable energy barrier associated with the bcc-fcc transformation mechanism via dislocation based theory is 402 mJm^{-2}, as revealed by the current atomistic calculations.

3.1. Modeling of the critical transformation stress τ_{crit}^{trans}

Consider the dislocation arrangement in Fig. 8. The applied stress, τ, aids the motion of $a_o/8<110>$ and $a/12<112>$ dislocations to form the fcc crystal in the region of intersection. Irrespective of the ordering of the shear process, we can write the total energy of the dislocation configuration in Fig. 8 as follows:

$$E_{total} = E_{int} + E_{self} + E_{\gamma}^{\{110\}} + E_{\gamma}^{\{111\}} - W \tag{4}$$

$$E_{total} = -\frac{\mu_{\{110\}<110>} b^2_{<110>}}{2\pi} \ln\left(\frac{d_1^{\{110\}}}{r_o}\right) - \frac{\mu_{\{111\}<112>} b^2_{<112>}}{2\pi} \ln\left(\frac{d_1^{\{110\}}}{r_o}\right) + \int_{-\infty}^{+\infty} \gamma_{\{110\}} f(x)dx + \int_{-\infty}^{+\infty} \gamma_{\{111\}} f(x)dx + \frac{N\mu_{\{110\}<110>} b^2_{<110>}}{2}\left(1-\nu\cos^2\theta\right) + \frac{\mu_{\{111\}<112>} b^2_{<112>}}{2}\left(1-\nu\cos^2\theta\right) - \sum_{i=1}^{N-1} \tau b_{<110>} d_i^{\{110\}} - \sum_{i=1}^{N-1} \tau b_{<112>} d_i^{\{111\}} \tag{5}$$

where E_{int} is the elastic energy due to the interaction of the dislocations, E_{self} is the line energy of the dislocation, $E_{\gamma}^{\{110\}}$ and $E_{\gamma}^{\{111\}}$ are the misfit energies which represent the periodic non-linear interatomic interactions of the dislocations on {110}<110> and {111}<112> systems respectively, and W is the work required to move the dislocations. Note that the sum of E_{self} and E_{int} represents the total elastic strain energy stored in the crystal. Similarly, μ is the shear modulus, and N is the number of dislocations participating in the transformation process. The terms $E_{\gamma}^{\{110\}}$ and $E_{\gamma}^{\{111\}}$ are periodic and depend on the position of the dislocation line within the lattice, and the parameter γ is the stacking fault energy landscape associated with the transformation. By considering the lattice discreteness, the misfit energy E_{γ}^{s} for the case of {110}<110> shear can be written as follows:

$$E_{\gamma}^{\{110\}} = \sum_{m=-\infty}^{+\infty} \gamma_{\{110\}} f(ma' - u)a' \tag{6}$$

where a^{I} is the periodicity of $E_{\gamma}^{\{110\}}$ and is defined as the shortest distance between two equivalent atomic rows in the direction of the dislocation displacement (Carrez et al., 2007; Joos and Duesbery, 1997; Joós et al., 1994; Lu et al., 2000; Schoeck,

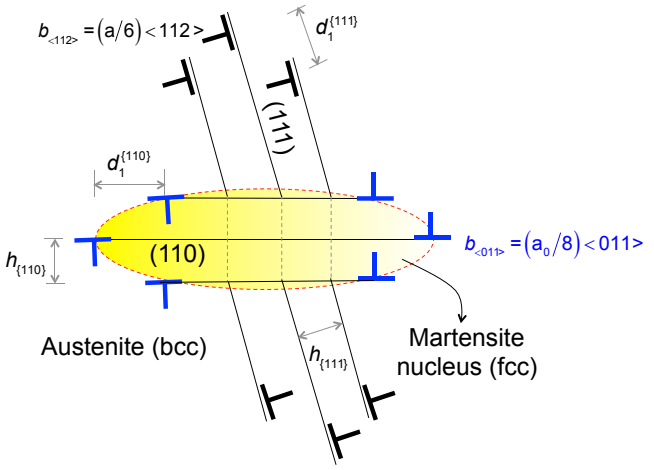

Fig. 8. The arrangement of dislocations during bcc-fcc martensitic transformation in FeMnAlNi alloy. The intersection of two sets of dislocations create a region containing the fcc crystal.

Please cite this article in press as: Ojha, A., Sehitoglu, H., Transformation stress modeling in new Fe–Mn–Al–Ni shape memory alloy, International Journal of Plasticity (2016), http://dx.doi.org/10.1016/j.ijplas.2016.08.003

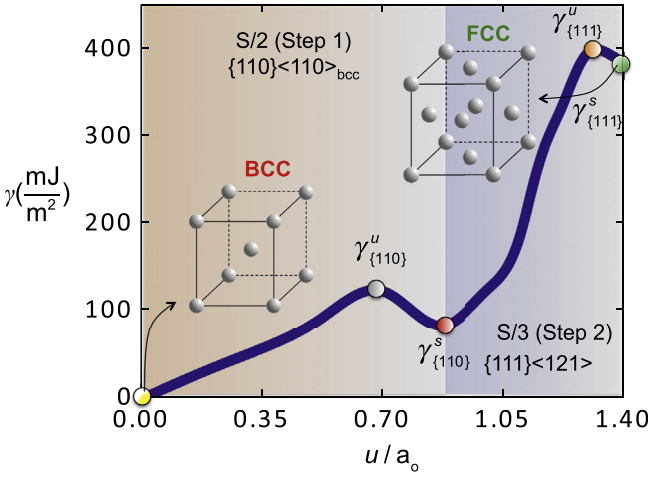

Fig. 9. Energy barrier profile (γ-curve) associated with bcc-fcc transformation via heterogeneous dislocation-based transformation mechanism in FeMnAlNi alloy.

2011). The misfit energy of {111}<112> shear can be obtained in a similar manner, as described in equation (6) by replacing $\gamma_{\{110\}}$ with $\gamma_{\{111\}}$. The solution to the disregistry function $f(x)$ in the dislocation core is (Joos and Duesbery, 1997; Ojha and Sehitoglu, 2014; Schoeck, 2011):

$$f(x) = \frac{b}{2} + \frac{b}{\pi}\left\{\tan^{-1}\left(\frac{x}{\xi}\right) + \tan^{-1}\left(\frac{x-d}{\xi}\right) + \tan^{-1}\left(\frac{x-2d}{\xi}\right) + \ldots + \tan^{-1}\left(\frac{x-(N-1)d}{\xi}\right)\right\} \tag{7}$$

where $\zeta = d/2(1-\nu)$ is the half-core width of the dislocation for an isotropic solid, d is the interplanar distance of the dislocation glide plane and υ is the Poisson's ratio.

In order to calculate the misfit energy term, E_γ, we fit the γ profile in Fig. 9 using the sine analytical functions, both for S/2 and S/3 shears. As an example, the fitting function in Fig. 9 is:

$$\begin{aligned}
&\gamma_{\{110\}}(f(x)) = \gamma^u_{\{110\}}\sin\left(\pi\frac{f(x)}{2}\right) \quad \text{for } 0 \le f(x) \le 0.7\\
&\gamma_{\{110\}}(f(x)) = \frac{1}{2}\left(\gamma^u_{\{110\}} + \gamma^s_{\{110\}}\right) + \left(\gamma^u_{\{110\}} - \frac{1}{2}\left(\gamma^u_{\{110\}} + \gamma^s_{\{110\}}\right)\right) \times \sin(2\pi(f(x) - 1.25)) \quad \text{for } 0.7 < f(x) \le 0.88
\end{aligned} \tag{8}$$

$$\begin{aligned}
&\gamma_{\{111\}}(f(x)) = \frac{1}{2}\left(\gamma^s_{\{110\}} + \gamma^u_{\{111\}}\right) + \left(\gamma^u_{\{111\}} - \frac{1}{2}\left(\gamma^u_{\{110\}} + \gamma^s_{\{110\}}\right)\right) \times \sin(2\pi(f(x))) \quad \text{for } 0.88 < f(x) \le 1.29\\
&\gamma_{\{111\}}(f(x)) = \frac{1}{2}\left(\gamma^s_{\{111\}} + \gamma^u_{\{111\}}\right) + \left(\gamma^u_{\{111\}} - \frac{1}{2}\left(\gamma^u_{\{111\}} + \gamma^s_{\{111\}}\right)\right) \times \cos(2\pi(f(x) - 1.25)) \quad \text{for } 1.29 < f(x) \le 1.40
\end{aligned} \tag{9}$$

Equation (8) represents the fitting function corresponding to Fig. 9 for the case of {110}<110> shear and equation (9) represents that of {111}<112> shear. The term $b_{<110>}$ is the Burgers vector of the dislocation associated with the {110}<110> shear and $b_{<112>}$ that of the {111}<112> shear. Upon substituting the expressions (8,9) into equation (5) and minimizing it with respect to $d_1^{\{110\}}$ and $d_1^{\{111\}}$ $\left(\frac{\partial E_{total}}{\partial d_1^{\{110\}}} = \frac{\partial E_{total}}{\partial d_1^{\{111\}}} = 0\right)$, we can numerically solve for the critical transformation stress. The critical transformation stress obtained using this methodology is 191 MPa (see Table 2). A complete list of parameters used in the calculation of the critical transformation stress is provided in Tables 1 and 3.

3.2. Generalized Planar Fault Energy and twinning in fcc martensite

In the case of superelastic response, the transformed fcc martensite may undergo twinning beyond the critical twinning stress, τ_{cr}^{twin} to accommodate the deformation. Twinning in fcc crystals occurs on {111} plane and along <112> direction, and the Burgers vector of the twinning partial is b_p = a/6<112>, where 'a' is the lattice constant of the fcc crystal. During the growth of the martensite, the partial dislocations associated with twinning (b_p = a/6<112>) have to overcome an energy barrier, termed the Generalized Planar Fault Energy (GPFE). The GPFE can be obtained by shearing the consecutive {111}

Please cite this article in press as: Ojha, A., Sehitoglu, H., Transformation stress modeling in new Fe–Mn–Al–Ni shape memory alloy, International Journal of Plasticity (2016), http://dx.doi.org/10.1016/j.ijplas.2016.08.003

Table 1
Lattice constant of bcc and fcc crystals of Fe-34 at.%Mn-15 at.%Al-7.1 at.%Ni alloy. The experimentally observed value is also reported.

Alloy	Lattice constant (Å) (fcc martensite)		Lattice constant (Å) (bcc austenite)	
	Theory (DFT, This study)	Experiment (Omori et al., 2011)	Theory (DFT, This study)	Experiment (Omori et al., 2011)
FeMnAlNi	3.65	3.672	2.88	2.903

Table 2
The critical twinning, τ_{crit}^{twin} and transformation stresses, τ_{crit}^{trans} for Fe-34 at.%Mn-15 at.%Al-7.1 at.%Ni alloy. The experimentally measured transformation stress value is also reported.

Alloy	Critical transformation stress (τ_{crit}^{trans}, MPa)		Critical twinning stress (τ_{crit}^{twin}, MPa)
	Theory (This study)	Experiment (Tseng et al., 2016)	Theory (This study)
FeMnAlNi	191	200	201

Table 3
The double shear energy parameters (in mJm^{-2}), the Burgers vectors of the dislocations associated with S/2 and S/3 shears ($b_{<112>}$ and $b_{<111>}$ in Å), the {111}<112> and {110}<110> shear moduli (in GPa), and the {110} and {111} interplanar distances ($d_{\{110\}}$ and $d_{\{111\}}$ in Å) associated with the dislocation based bcc-fcc transformation mechanism in FeMnAlNi alloy.

Material	$\gamma^{u}_{\{110\}}$ (mJm^{-2})	$\gamma^{s}_{\{110\}}$ (mJm^{-2})	$\gamma^{u}_{\{111\}}$ (mJm^{-2})	Burgers vector, S/2 shear ($b_{<112>}$, Å)	Burgers vector, S/3 shear ($b_{<111>}$, Å)	$\mu_{\{111\}<112>}$ (GPa)	$\mu_{\{110\}<110>}$ (GPa)	$d_{\{110\}}$ (Å)	$d_{\{111\}}$ (Å)
FeMnAlNi	124	82	398	0.51	1.5	16	12	2.03	2.10

planes each by a displacement equal to the Burgers vector of the twinning partial. In Fig. 10 (a), we consider a schematic of an undeformed fcc crystal oriented along the x = $[\bar{2}11]$, y = [111] and z = $[01\bar{1}]$ directions while Fig. 10(b) and (c) show the entire process of forming a twin through consecutive shearing of the {111} plane along the <112> direction. The energy cost per unit area corresponding to the formation of a twin can be quantified employing DFT simulations. We show the energy values corresponding to the faulted structures in the form of a GPFE curve as illustrated in Fig. 11. The number of {111} layers used for the calculation is 13, which is sufficient to obtain the converged energy values. It is worth pointing out that the large simulation cell eliminates the effect of free surfaces on the calculated energy parameters shown in the GPFE curve. In Fig. 11, the term γ_{us} represents the energy barrier required to nucleate the first layer-stacking fault. Similarly, the term γ_{ut} represents the energy barrier required to grow the twin, $2\gamma_{tsf}$ represents the stable energy fault corresponding to the 2nd layer fault, and γ_{tbm} is the twin boundary migration energy given by $\gamma_{tbm} = \gamma_{ut} - 2\gamma_{tsf}$. It should be noted that after the formation of the three layer stacking fault, the energy values associated with the GPFE curve stabilize in fcc crystals, including FeMnAlNi alloy (see Table 4).

We have developed the twinning stress model earlier using modified PN formalism (Ojha and Sehitoglu, 2014, 2016c; Wang and Sehitoglu, 2013). Consider the dislocation arrangement of a twin as shown in Fig. 12. The total energy of the dislocation configuration can be written as follows:

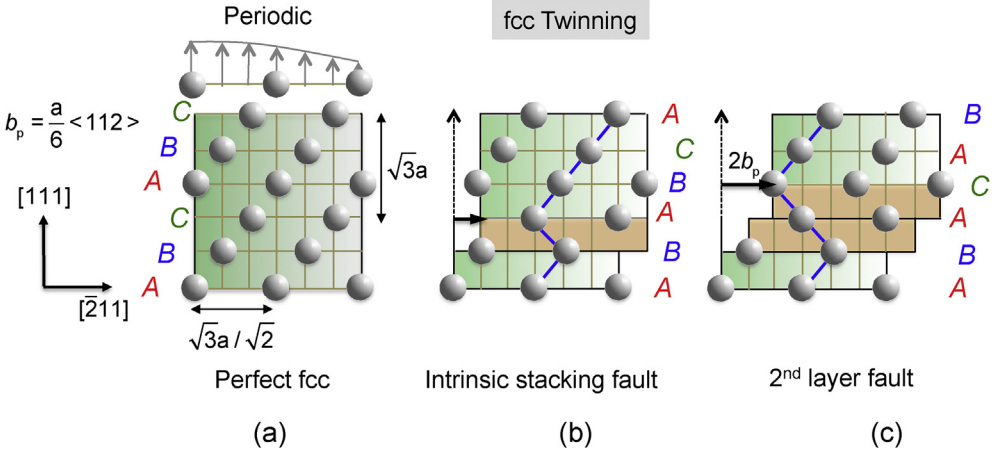

Fig. 10. Schematic of twin formation in an fcc crystal. (a) The twin system is {111}<112>, and the Burgers vector of the twinning partial is b_p = a/6<112> (b) the formation of an intrinsic stacking fault by the passage of b_p (c) the formation of a 2nd layer fault.

Please cite this article in press as: Ojha, A., Sehitoglu, H., Transformation stress modeling in new Fe–Mn–Al–Ni shape memory alloy, International Journal of Plasticity (2016), http://dx.doi.org/10.1016/j.ijplas.2016.08.003

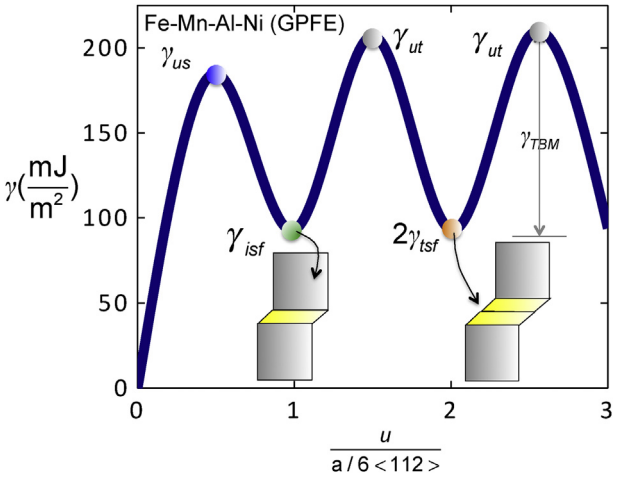

Fig. 11. The Generalized Planar Fault Energy (GPFE) of fcc FeMnAlNi alloy.

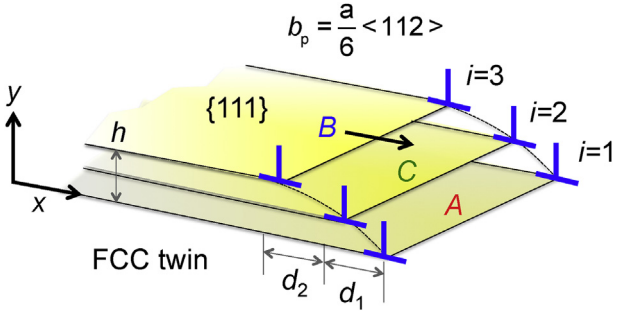

Fig. 12. Schematic of a twin nucleus in an fcc crystal.

$$E_{total} = E_{int} + E_{\gamma} + E_{line} - W \tag{10}$$

where E_{int} is the interaction energy of the dislocations, E_{γ} is the misfit energy associated with the dislocations comprising the twin, E_{line} is the dislocation line energy, and W is the externally applied stress. The term E_{γ} can be obtained by incorporating the GPFE curve expressed as the sum of sinusoidal functions with the dislocation distribution on the twin plane, commonly referred to as the disregistry function. The disregistry function associated with multiple dislocations on the twin plane can be written as follows (Joos and Duesbery, 1997; Ojha and Sehitoglu, 2014; Schoeck, 2011):

$$f(x) = \frac{b}{2} + \frac{b}{\pi}\left\{\tan^{-1}\frac{x}{\xi} + \tan^{-1}\frac{x-d_1}{\xi} + \tan^{-1}\frac{x-(d_1+d_2)}{\xi}\right\} \tag{11}$$

where x is the position of the dislocation line, d_1 and d_2 are the separation distances between the twinning dislocations and ξ is the half core width ratio determined as $d_{\{111\}}/2(1\text{-}\vartheta)$. The term $d_{\{111\}}$ is the {111} interplanar distance and ϑ is the Poisson ratio of the crystal. The misfit energy across a glide plane is defined as the sum of misfit energies between pairs of atomic planes and can be obtained from the GPFE as follows:

$$E_{\gamma} = \int_{-\infty}^{+\infty} \gamma_{GPFE}(f(x))dx \tag{12}$$

The integral form of misfit energy in equation (12) can be modified to discrete form to account for the variation of the disregistry as the dislocation moves infinitesimally from one position to the other along the twin interface. The discrete form of the misfit energy can be written as follows (Joos and Duesbery, 1997; Ojha and Sehitoglu, 2014; Schoeck, 2011):

Please cite this article in press as: Ojha, A., Sehitoglu, H., Transformation stress modeling in new Fe–Mn–Al–Ni shape memory alloy, International Journal of Plasticity (2016), http://dx.doi.org/10.1016/j.ijplas.2016.08.003

$$E_\gamma = \sum_{-\infty}^{+\infty} \gamma_{GPFE}(f(ma' - u))a' \tag{13}$$

The Peierls stress required to move the twinning dislocation can be obtained by taking the maximum slope of the misfit energy curve with respect to the dislocation position as follows:

$$\tau_p = \frac{1}{b}\max\left(\frac{\partial E_\gamma}{\partial u}\right) \tag{14}$$

It should be noted that the misfit energy does not account for the total elastic interactions comprising the twin, and therefore, the total energy expression that incorporates the elastic interactions of the dislocations is required to obtain the accurate twinning stress. To do so, we substitute each of the energy terms in equation (10) as follows:

$$E_{total} = -\frac{\mu_{\{111\}<112>}}{2\pi}\left(\ln\frac{d_1}{r_o} + \ln\frac{d_2}{r_o} + \ln\frac{d_1+d_2}{r_o}\right) + \sum_{m=-\infty}^{m=+\infty} \gamma_{GPFE}(f(ma' - u))a' + N\frac{\mu_{\{111\}<112>}b^2}{2(1-\nu)}\left(1 - \nu\cos^2\theta\right) + \sum_{i=1}^{2} \tau s h_{\{111\}} d_i \tag{15}$$

Here, $h_{\{111\}}$ is the height of the twin nucleus, s is the twinning shear defined as $b/d_{\{111\}}$ where $d_{\{111\}}$ is the {111} interplanar distance, r_o is the core width determined as $d_{\{111\}}/(1\text{-}\vartheta)$, and θ is the angle between the dislocation line and unit cell axes. The twinning stress is then obtained by minimizing the total energy with respect to the dislocation positions, d_1 and d_2 as follows:

$$\frac{\partial E_{total}}{\partial d_1} = \frac{\partial E_{total}}{\partial d_2} = 0 \tag{16}$$

Upon solving the set of equations (16), we obtain the CRSS for twinning as the minimum value of τ that satisfies both of these equations. The twinning stress, $\tau_{\text{crit}}^{\text{twin}}$ obtained using equation (16) utilizing the parameters provided in Table 4 is 201 MPa, and is reported in Table 2.

3.3. Slip stress calculation in bcc and fcc FeMnAlNi

It is well known that slip curtails reversibility in shape memory alloys due to permanent plastic strain accumulation during phase transformation (Norfleet et al., 2009; Ojha and Sehitoglu, 2016a; Sehitoglu et al., 2001, 2002; Simon et al., 2010). Therefore, slip resistance should be higher compared to the transformation/twinning stress for better superelastic behavior and functionality. In this section, we develop a PN based theoretical model to calculate the slip stress in both bcc austenite and fcc martensite in FeMnAlNi alloy by incorporating the Generalized Stacking Fault Energy (GSFE). The GSFE is the energy barrier per unit area required to nucleate a slip, and can be obtained by rigidly shearing one half of the crystal with respect to other half by a displacement of $u = nb$ where n is a constant ranging from 0 to 1, and b is the Burgers vector of the slip dislocation. Slip occurs on {110}<111>, {112}<111> and {123}<111> systems in a bcc crystal and {111}<110> system in an fcc crystal. The Burgers vector of the slip dislocation in bcc and fcc crystal are $b_{\text{bcc}} = a_0/2<111>$ and $b_{\text{fcc}} = a/2<110>$ respectively where 'a_0' and 'a' are the lattice constants of the bcc and fcc crystals respectively. In Table 5, we show the relevant energy parameters associated with the {110}<111> bcc and {111}<110> fcc slip systems.

Table 4
The energy parameters of the GPFE curve (in mJm^{-2}), the {111}<112> shear modulus ($\mu_{\{111\}<112>}$ in GPa), the Burgers vector of the twinning partial (b in Å), the {111} interplanar distance ($d_{\{111\}}$ in Å) and the twinning shear (s) associated with twinning in FeMnAlNi fcc martensite.

Material	γ_{us} (mJm^{-2})	γ_{isf} (mJm^{-2})	γ_{ut} (mJm^{-2})	$2\gamma_{tsf}$ (mJm^{-2})	$\mu_{\{111\}<112>}$ (GPa)	Burgers vector (b, Å)	$d_{\{111\}}$ (Å)	Twinning shear (s)
FeMnAlNi	185	98	207	93	16	1.5	2.1	0.71

Table 5
The energy parameters of the GSFE curve (in mJm^{-2}), the shear moduli, the Burgers vector of the slip dislocation (b in Å) associated with slip in bcc and fcc FeMnAlNi alloy.

Material	BCC Austenite				FCC Martensite				
	γ_{us}^{bcc} (mJm^{-2})	b_{bcc} (Å)	$\mu_{\{110\}<111>}$ (GPa)	$\tau_{crit.bcc}^{slip}$ (MPa)	γ_{us}^{fcc} (mJm^{-2})	γ_{isf} (mJm^{-2})	b_{fcc} (Å)	$\mu_{\{111\}<112>}$ (GPa)	$\tau_{crit.bcc}^{slip}$ (MPa)
FeMnAlNi	281	2.5	14	393	185	64	1.5	16	335

Please cite this article in press as: Ojha, A., Sehitoglu, H., Transformation stress modeling in new Fe–Mn–Al–Ni shape memory alloy, International Journal of Plasticity (2016), http://dx.doi.org/10.1016/j.ijplas.2016.08.003

Fig. 13 shows the GSFE curve for {110}<111> bcc and {111}<110> fcc slip systems. A full a/2<110> dislocation in an fcc crystal dissociates into two partial dislocations as follows:

$$\frac{a}{2}\left[\bar{1}10\right] \rightarrow \frac{a}{6}\left[\bar{1}2\bar{1}\right] + \frac{a}{2}\left[\bar{2}11\right]$$

The term γ_{us}^{fcc} is the unstable stacking fault energy, and γ_{isf} is the stable intrinsic stacking fault energy in an fcc crystal. The two dissociated partial dislocations are separated by an intrinsic stacking fault. It is important to note that dislocation in a bcc crystal, however, does not attain a metastable structure during rigid shearing of the crystal, and thus no dissociation occurs. Our previous theoretical calculations in bcc metals have shown that higher the γ_{us}, higher is the slip nucleation stress (Ojha and Sehitoglu, 2016b). We also obtained the γ_{us} values of 301 and 327 mJm^{-2} for {112}<111> slip in twinning and anti-twinning sense respectively, and 298 mJm^{-2} for {123}<111> systems in the current work. Due to the lower γ_{us} value of {110}<111> system compared to other systems, the {110}<111> system is likely to be activated in FeMnAlNi alloy.

The critical slip stress formulation can be developed using modified Peierls Nabarro formalism in a similar manner as described earlier. The misfit energy function associated with slip can be written as follows:

$$E_{\gamma}^{slip} = \sum_{m=-\infty}^{m=+\infty} \gamma_{GSFE}(f(ma' - u))a' \tag{17}$$

where γ_{GSFE} is the GSFE energy landscape expressed in sinusoidal form, and f(x) is the disregistry function. The disregistry function for the case of slip dislocation in a bcc crystal can be written as follows:

$$f(x) = \frac{b}{\pi}\left(\tan^{-1}\left(\frac{x}{\zeta}\right)\right) + \frac{b}{2} \tag{18}$$

where the terms have been described earlier in equations (12–14). The misfit energy and the disregistry function for the case of a dissociated dislocation in an fcc crystal can be obtained in a similar manner as described in equation (12). The critical slip stress can now be obtained as the maximum slope of the misfit energy variation with the dislocation position as follows:

$$\tau_{crit}^{slip} = \frac{1}{b}\max\left(\frac{\partial E_{\gamma}^{slip}}{\partial u}\right) \tag{19}$$

By substituting the parameters provided in Table 5 into equation (19), the critical slip stresses for bcc austenite and fcc martensite are obtained as 393 and 335 MPa respectively.

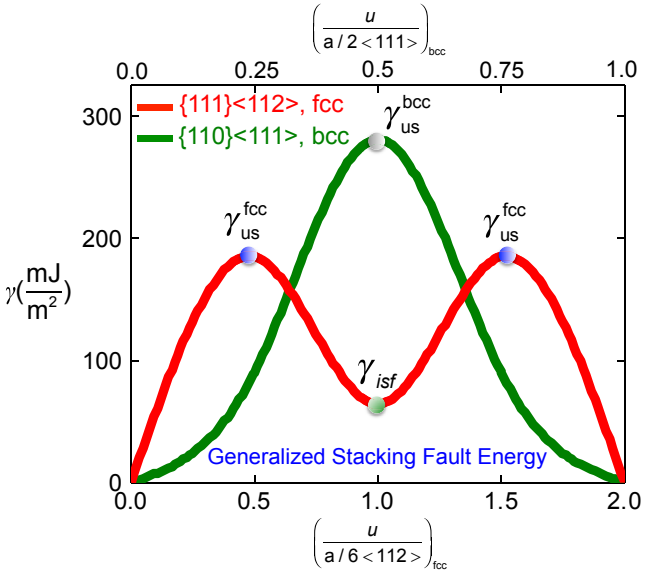

Fig. 13. The Generalized Stacking Fault Energy (GSFE) associated with bcc austenite and fcc martensite slips in FeMnAlNi alloy.

Please cite this article in press as: Ojha, A., Sehitoglu, H., Transformation stress modeling in new Fe–Mn–Al–Ni shape memory alloy, International Journal of Plasticity (2016), http://dx.doi.org/10.1016/j.ijplas.2016.08.003

4. Discussion of the results

4.1. Transformation energies and the path of bcc-fcc transformation

Upon comparing the energetics of the bcc-fcc transformation in FeMnAlNi alloy (Figs. 7 and 9), we observe that heterogeneous double shear mechanism proceeds with a much lower energy barrier compared to Bain distortion, and hence is the favorable pathway in FeMnAlNi alloy. The critical transformation stress obtained by incorporating the double shear energy with the Peierls Nabarro approach yields a value of 191 MPa, which is close to the experimental value of 200 MPa. Concurrently, we also obtain the energy barrier associated with the martensite twinning in the form of GPFE, and subsequently predict the twinning stress as 201 MPa. Similarly, the unstable fault energies (γ_{us}) corresponding to the austenite slip is 281 mJm^{-2} and that of the martensite slip is 185 mJm^{-2}. These two values of unstable fault energies yield the critical slip stresses of 393 MPa and 335 MPa respectively for bcc austenite and fcc martensite. We note that the twinning stress value for FeMnAlNi alloy is higher than the transformation stress, but much lower than slip stresses. Overall, a higher slip resistance compared to the twinning or transformation stresses in FeMnAlNi alloy ensures minimum plastic strain accumulation and higher strain recoverability. It is worth emphasizing that during the calculation of the transformation stress, the order of shearing does not affect the result.

If we carefully investigate the energy pathway associated with the bcc-fcc transformation mechanism shown in Fig. 9, two distinct features are noted: (i) First, the shear, S/2, on the {110} plane in <110> direction progresses with a much lower energy barrier compared to the shear on {111} plane in <112> direction. The S/2 shear attains a stable energy value after which the energy rapidly increases with an increase in S/3 shear on the {111} plane. (ii) Second, the increase in energy upon shearing {111} planes shows rather uneven profile before attaining the stable fcc phase. This may be a result of the atomic movements during relaxation, as the pure shear alone on the {111} plane is expected to yield an energy profile often approximated by a sinusoidal function. In the present analysis, we found that the S/3 shear is accompanied with dilatations of 0.22 Å normal to the {111} plane. In summary, pure shear alone cannot form the exact fcc crystal from the bcc phase and should be accompanied with local atomic relaxation, as validated by our simulation results.

Early works on martensitic transformation considered the role of dislocations for the bcc-fcc transformation (Olson and Cohen, 1976a, b). The dislocation based shear mechanism employed in the current work is a further extension to Bogers Burgers double shear mechanism (Bogers and Burgers, 1964) whereby dislocations accomplish two simultaneous shears of $a_0/8<110>$ and $a/12<112>$ leading to an fcc structure. In this context, since the transformation is accomplished by the intersection of dislocations, the current mechanism is referred to as heterogeneous transformation mechanism unlike the homogeneous Bain transformation. As noted earlier, the double shears required for bcc-fcc transformation are achieved by the passage of $a_0/8<110>$ dislocations on every second {110} plane (S/2 shear) and $a/12<112>$ dislocations on every third {111} plane (S/3 shear). The intersection of these two sets of dislocations generates a region containing the exact fcc crystal. In fact, these dislocations have been shown to be the precursors in martensitic transformation in other bcc metals and alloys as well, as validated by molecular dynamics simulations (Sinclair and Hoagland, 2008).

4.2. Role of solute segregation

The role of solute segregation cannot be neglected in the present case owing to four different elements comprising FeMnAlNi alloy. The role of solute segregation in decreasing the stacking fault energy has been well documented in the literature (Finkenstadt and Johnson, 2006; Ojha and Sehitoglu, 2014; Suzuki, 1962). In order to assess the potential solute segregation effects, we systematically checked the role of solute positions on the intrinsic stacking fault energy by simultaneously varying the element type and the compositions therein. In the present case, we note that the presence of Mn atoms are favored near the fault compared to all other elements thereby reducing the intrinsic stacking fault energy by approximately 32% (144–98 mJm^{-2}) when compared to the presence of Mn atoms away from the fault (Fig. 14). In this case, the intrinsic stacking fault energy reported in Fig. 11, and the transformation energy path in Fig. 9 correspond to the lowest structural energies.

4.3. The role of slip strength

We note that the austenite and martensite slip stresses of FeMnAlNi are substantially higher (approximately by 95%) compared to both the transformation and twinning stress levels. The importance of high slip resistance compared to the transformation and twinning stresses has been well recognized in other shape memory alloys as well (Norfleet et al., 2009; Ojha and Sehitoglu, 2016a; Sehitoglu et al., 2001, 2002; Simon et al., 2010). It has been observed that slip dislocations nucleate during transformation process due to the high internal stresses and strains along the austenite/martensite interfaces (Sun et al., 1999). The issue with austenite or martensite slips during crystallographic phase transformation is their contribution to hysteresis, thus degrading the functionality of SMAs. Slip mediated plasticity is found to interact with the austenite–martensite interface, and increase the resistance of the martensite interfacial motion during phase transformation process. In other words, they stabilize the martensite with cycling. Experiments (Krooß et al., 2015) have shown that high density of dislocations are observed along the austenite/martensite interface to accommodate the incompatibility. These dislocations are found to pin the interface thereby restricting the motion of martensite interfaces, and resulting in a much lower strain

Please cite this article in press as: Ojha, A., Sehitoglu, H., Transformation stress modeling in new Fe–Mn–Al–Ni shape memory alloy, International Journal of Plasticity (2016), http://dx.doi.org/10.1016/j.ijplas.2016.08.003

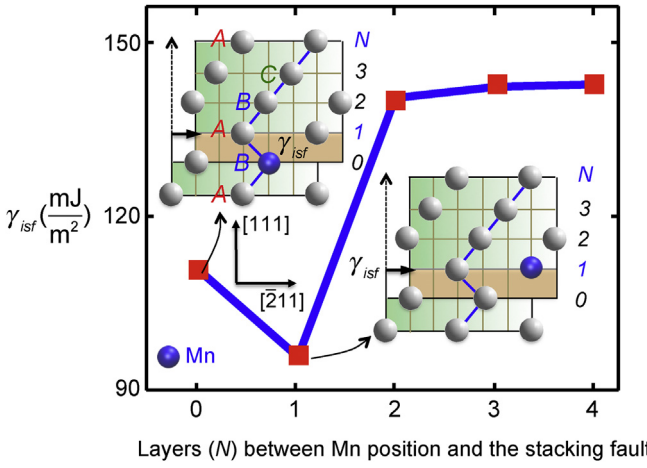

Fig. 14. Solute segregation effect observed in FeMnAlNi alloy as a function of the position of Mn atoms away from the fault.

recoverability compared to the theoretically derived transformation strains. Most changes occur within the first ten cycles and limit the utilization of shape memory alloys. For example, in some of the Ti-based alloys (Ti-24 at.%Zr-13 at.%Nb) (Kim et al., 2015), the critical stress for martensite slip is lower than the twinning stress, and such alloys do not exhibit superelasticity, as validated by experiments and our recent theoretical calculation (Ojha and Sehitoglu, 2016b). In such a case of low slip stress, it is easier to deform by slip than twinning, thus contributing to plastic strain accumulation and almost no recoverability. Our calculations on FeMnAlNi alloy show that the slip stresses in both austenite and martensite are approximately 95% higher than the twinning or the transformation stresses. Based on these results presented in this work, the FeMnNiAl has the potential to show resistance to cyclic degradation.

4.4. Maximum transformation strains

The maximum theoretical strains can also be obtained utilizing lattice deformation theory (LDT). The LDT assumes that the total transformation strain is achieved by the change in lattice constants during austenite to martensitic transformation. The details of the LDT are presented elsewhere (Bhattacharya, 2003; Saburi and Nenno, 1981). In the case of tension, high transformation strain of approximately 25% is obtained while in the case of compression, the maximum theoretical strain is obtained to be approximately 11%, as depicted in Fig. 15. However, experimental observations are reported to be in contrary to the transformation strain values obtained theoretically. The maximum transformation strain obtained theoretically for the case of [100] tension is 5% while that in compression is 3%. A detail analysis suggested that the poor recoverability compared to theoretical calculations in FeMnAlNi alloy is due to the presence of the retained martensite (Tseng et al., 2015b, 2016). Upon TEM investigations, it was shown that the austenite and the austenite–martensite interfaces contained

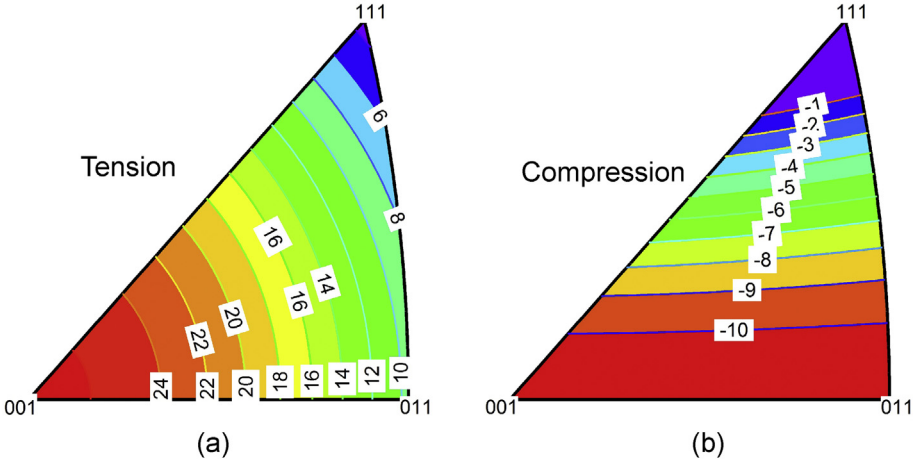

Fig. 15. Orientation dependence of transformation strains for FeMnAlNi in (a) tension and (b) compression.

Please cite this article in press as: Ojha, A., Sehitoglu, H., Transformation stress modeling in new Fe–Mn–Al–Ni shape memory alloy, International Journal of Plasticity (2016), http://dx.doi.org/10.1016/j.ijplas.2016.08.003

dislocations that curtailed the reversibility, while no such dislocations were found for the samples subjected to compressive deformation. Similarly, the effect of the B2 precipitates and aging time has been investigated in FeMnAlNi (Tseng et al., 2015a). It was observed that the transformation temperatures decreased with an increase in aging time and temperature, while the effect on recoverable strain had no such relationship. In fact, the recoverable strains increased with an increase in time, approximately from 3.6% to 7.2% with an increase in aging time from zero to four hours and decrease to 2.5% after prolonged aging time (approximately 10 h) (Tseng et al., 2015b, 2016). It is important to note that our calculations do not incorporate the effect of precipitates on the twinning and transformation stress, and hence is applicable to FeMnAlNi alloy with homogeneous microstructure.

4.5. The orientation relationship between austenite and martensite

Recently, the role of dislocations in accomplishing the martensitic transformation has been validated using high-resolution TEM investigations (Yang et al., 2014). In this regard, the orientation relationship between the transformed martensite phase and the parent austenite phase is an important topic to investigate, which has been extensively discussed in the literature (Sinclair and Hoagland, 2008; Yang et al., 2014). The orientation relationship between the bcc and the fcc matrix has been studied utilizing experiments and atomistic simulations. While one set of several experimental observations have shown that the orientation relationship between the fcc and the bcc matrix follows Kurdjumov-Sachs (KS) relationship (Yang et al., 2014), the atomistic simulations have shown that the orientation relationship between the two is Pitsch (Sinclair and Hoagland, 2008), similar to the orientation relationship we obtain in the current work via dislocation based transformation mechanism. It has been argued that the difference between these two observations may be a result of the inaccuracy of the orientation measurements (Sinclair and Hoagland, 2008). It is important to point out that the following crystallographic orientation relationship exists between the bcc and fcc crystals in Pitsch orientation relationship:

$$[011]_{\text{fcc}} \| [111]_{\text{bcc}},\ \left[01\bar{1}\right]_{\text{fcc}} \| \left[2\bar{1}\bar{1}\right]_{\text{bcc}},\ \left[\bar{1}00\right]_{\text{fcc}} \| \left[01\bar{1}\right]_{\text{bcc}}$$

We note that the double shears yield a close Pitsch orientation relationship between the parent bcc and the transformed fcc crystal. In the case of Bogers Burgers homogeneous shear mechanism, it has been originally discussed that an additional dilatation of 3.6% is required normal to the $\{111\}_{\text{fcc}}$ shear plane to attain the exact bcc crystal with correct lattice constant and Pitsch orientation relationship with respect to the parent fcc crystal. As discussed earlier, the S/3 shear in the current mechanism is associated with dilatations of 0.22Å normal to the {111} shear plane. This dilatational component is required to form the correct {111} stacking and the {111} interplanar distance of the fcc crystal, and thus to achieve a Pitsch orientation relationship with the parent bcc crystal.

It is important to point out that the current theoretical model for critical transformation stress is formulated by considering the total energy of the region/volume of the crystal in which a bcc phase undergoes transformation to the martensite fcc nucleus. In experimental sense, this region/volume can be considered as the localized region/volume of the crystal with specific energy (given by expression (5) in the paper) where bcc to fcc transformation first initiates at the CRSS level. It is also worth pointing out that within the total energy formulation (5) for transformation, the misfit energy term ($E_{misfit} = \int_{-\infty}^{+\infty} \gamma(f(x))dx$) associated with $S/2$ and $S/3$ shears accurately represent the localized energy variation associated with the non-linear atomic interactions during transformation. The energy variations appearing in the form of peaks and valleys in the γ-curve (Fig. 9) represent unstable and metastable positions (local energy features) associated with the Bogers-Burgers double shear mechanism.

In summary, the advantage of using FeMnAlNi alloy compared to other shape memory alloys is the dominance of iron which is less costly compared to Ni and Ti, the higher moduli, and higher slip stress relative to transformation stress. In this regard, the FeMnAlNi alloy has potential applications for a wider temperature range as the M_d temperature is significantly above A_f. In this study, we established the several parameters such as transformation stress and twinning stress that govern the superelastic effect in FeMnAlNi alloy. In order to understand the mechanical response, it is crucial to determine these quantities accurately, and therefore, a theoretical work encompassing several parameters such as shear modulus, lattice constant, and unstable energy values is demanding. It is important to note that the determination of these quantities using experiments requires tremendous efforts, and atomistic simulations prove useful which is the approach in our present study.

5. Conclusions

The following conclusion are drawn from the current paper:

(1) We obtain the bcc-fcc transformation energy profiles associated with the Bain deformation and the dislocation based heterogeneous transformation mechanism (Bogers-Burgers type) utilizing first principles density functional theory (DFT) calculations. Our calculations show that the heterogeneous martensitic transformation mechanism proceeds with a much lower energy barrier compared to the Bain deformation in FeMnAlNi alloy.

Please cite this article in press as: Ojha, A., Sehitoglu, H., Transformation stress modeling in new Fe–Mn–Al–Ni shape memory alloy, International Journal of Plasticity (2016), http://dx.doi.org/10.1016/j.ijplas.2016.08.003

(2) The theoretical model for bcc-fcc transformation is developed on Peierls Nabarro framework by incorporating the energetics associated with the dislocation based transformation mechanism with the elastic interactions of the dislocations. The critical transformation value obtained theoretically is 191 MPa, which is close to the experimental value of approximately 200 MPa.
(3) The critical twinning stress of 201 MPa for fcc martensite in FeMnAlNi is obtained using PN approach by incorporating misfit energies and the twinning energy barrier (GPFE) associated with the dislocations comprising the twin.
(4) Our calculations show that the second shear, S/3 associated with {111}<112> dislocations is accompanied with dilatations of 0.22 Å normal to the shear plane. In this regard, pure shear should be coupled with local atomic relaxation to form the exact fcc crystal.
(5) The maximum theoretical transformation strains of 26% and 11% are obtained in [001] oriented sample in tension and compression respectively, as revealed by lattice deformation theory (LDT) calculations.
(6) To address the effect of solute segregation, we note that the presence of Mn atoms are favored near the fault reducing the intrinsic stacking fault energy by approximately 32% when compared to the case where Mn atoms are away from the fault.

Acknowledgements

The work is supported by Nyquist Chair Funds and by NSF CMMI grant 13-00284 which are gratefully acknowledged.

References

Ahmed, T., Rack, H.J., 1996. Martensitic transformations in Ti-(16–26 at%) Nb alloys. J. Mater. Sci. 31, 4267–4276.
Ando, K., Omori, T., Ohnuma, I., Kainuma, R., Ishida, K., 2009. Ferromagnetic to weak-magnetic transition accompanied by bcc to fcc transformation in Fe-Mn-Al alloy. Appl. Phys. Lett. 95, 2504.
Bhattacharya, K., 2003. Microstructure of Martensite: Why it Forms and How it Gives Rise to the Shape-memory Effect. Oxford University Press.
Bogers, A.J., Burgers, W.G., 1964. Partial dislocations on the {110} planes in the BCC lattice and the transition of the FCC into the BCC lattice. Acta Metall. 12, 255–261.
Bowles, J.S., Mackenzie, J.K., 1954. The crystallography of martensite transformations I. Acta Metall. 2, 129–137.
Burgers, W.G., 1934. On the process of transition of the cubic-body-centered modification into the hexagonal-close-packed modification of zirconium. Physica 1, 561–586.
Carrez, P., Ferré, D., Cordier, P., 2007. Peierls–Nabarro model for dislocations in MgSiO3 post-perovskite calculated at 120 GPa from first principles. Philos. Mag. 87, 3229–3247.
Christian, J.W., 2002. The Theory of Transformations in Metals and Alloys. Newnes.
Duerig, T.W., Melton, K.N., Stockel, D., Wayman, C.M., 1990. Engineering aspects of shape memory alloys. Butter worth-Heinemam, London.
Efstathiou, C., Sehitoglu, H., Carroll, J., Lambros, J., Maier, H.J., 2008. Full-field strain evolution during intermartensitic transformations in single-crystal NiFeGa. Acta Mater. 56, 3791–3799.
Ezaz, T., Sehitoglu, H., Abuzaid, W., Maier, H.J., 2012. Higher order twin modes in martensitic NiTi—The (201) case. Mater. Sci. Eng. A 558, 422–430.
Ezaz, T., Sehitoglu, H., Maier, H.J., 2011. Energetics of twinning in martensitic NiTi. Acta Mater. 59, 5893–5904.
Ezaz, T., Wang, J., Sehitoglu, H., Maier, H.J., 2013. Plastic deformation of NiTi shape memory alloys. Acta Mater. 61, 67–78.
Finkenstadt, D., Johnson, D.D., 2006. Solute/defect-mediated pathway for rapid nanoprecipitation in solid solutions: γ surface analysis in fcc Al-Ag. Phys. Rev. B 73, 024101.
Gall, K., Sehitoglu, H., 1999. The role of texture in tension–compression asymmetry in polycrystalline NiTi. Int. J. Plasticity 15, 69–92.
Gall, K., Sehitoglu, H., Chumlyakov, Y.I., Kireeva, I.V., 1998. Pseudoelastic cyclic stress-strain response of over-aged single crystal Ti-50.8 at% Ni. Scr. Mater. 40, 7–12.
Gall, K., Sehitoglu, H., Chumlyakov, Y.I., Kireeva, I.V., 1999. Tension–compression asymmetry of the stress–strain response in aged single crystal and polycrystalline NiTi. Acta Mater. 47, 1203–1217.
Hamilton, R.F., Sehitoglu, H., Chumlyakov, Y., Maier, H.J., 2004. Stress dependence of the hysteresis in single crystal NiTi alloys. Acta Mater. 52, 3383–3402.
Ibarra, A., San Juan, J., Bocanegra, E.H., Nó, M.L., 2007. Evolution of microstructure and thermomechanical properties during superelastic compression cycling in Cu–Al–Ni single crystals. Acta Mater. 55, 4789–4798.
Joos, B., Duesbery, M.S., 1997. The Peierls stress of dislocations: an analytic formula. Phys. Rev. Lett. 78, 266.
Joós, B., Ren, Q., Duesbery, M.S., 1994. Peierls-Nabarro model of dislocations in silicon with generalized stacking-fault restoring forces. Phys. Rev. B 50, 5890–5898.
Kim, H.Y., Fu, J., Tobe, H., Kim, J.I., Miyazaki, S., 2015. Crystal structure, transformation strain, and superelastic property of Ti–Nb–Zr and Ti–Nb–Ta alloys. Shape Mem. Superelast. 1, 107–116.
Kokorin, V.V., Gunko, L.P., Shevchenko, O.M., 1993. Martensitic γ ⇄ α transformation in ausaged Fe-Co based alloys. Scr. metall. mater. 28, 35–40.
Kresse, G., Furthmüller, J., 1996. Efficient iterative schemes for ab-initio total-energy calculations using a plane-wave basis set. Phys. Rev. B 54, 11169–11186.
Koval, Y.U.N., Kokorin, V.V., Khandros, L.G., 1979. The Shape-Memory Effect in Iron–Nickel–Cobalt–Titanium Alloys. Fiz. Met. Metalloved 48, 1309–1311.
Kresse, G., Hafner, J., 1993. Ab initio molecular dynamics for open-shell transition metals. Phys. Rev. B 48, 13115–13118.
Krooß, P., Niendorf, T., Kadletz, P.M., Somsen, C., Gutmann, M.J., Chumlyakov, Y.I., Schmahl, W.W., Eggeler, G., Maier, H.J., 2015. Functional fatigue and tension–compression asymmetry in [001]-Oriented Co49Ni21Ga30 high-temperature shape memory alloy single crystals. Shape Mem. Superelast. 1, 6–17.
Lagoudas, D.C., 2008. Shape Memory Alloys: Modeling and Engineering Applications. Springer Science & Business Media.
Lagoudas, D.C., Entchev, P.B., 2004. Modeling of transformation-induced plasticity and its effect on the behavior of porous shape memory alloys. Part I: constitutive model for fully dense SMAs. Mech. Mater. 36, 865–892.
Lu, G., Kioussis, N., Bulatov, V.V., Kaxiras, E., 2000. The peierls-nabarro model revisited. Philos. Mag. Lett. 80, 675–682.
Mackenzie, J.K., Bowles, J.S., 1954. The crystallography of martensite transformations II. Acta Metall. 2, 138–147.
Maki, T., Furutani, S., Tamura, I., 1989. Shape memory effect related to thin plate martensite with large thermal hysteresis in ausaged Fe-Ni-Co-Ti alloy. ISIJ Int. 29, 438–445.
Miyazaki, S., Otsuka, K., 1989. Development of shape memory alloys. ISIJ Int. 29, 353–377.
Moumni, Z., Zaki, W., Nguyen, Q.S., 2008. Theoretical and numerical modeling of solid–solid phase change: application to the description of the thermomechanical behavior of shape memory alloys. Int. J. Plasticity 24, 614–645.
Nishiyama, Z., 2012. Martensitic Transformation. Elsevier.

Please cite this article in press as: Ojha, A., Sehitoglu, H., Transformation stress modeling in new Fe–Mn–Al–Ni shape memory alloy, International Journal of Plasticity (2016), http://dx.doi.org/10.1016/j.ijplas.2016.08.003

Norfleet, D.M., Sarosi, P.M., Manchiraju, S., Wagner, M.-X., Uchic, M.D., Anderson, P.M., Mills, M.J., 2009. Transformation-induced plasticity during pseudoelastic deformation in Ni–Ti microcrystals. Acta Mater. 57, 3549–3561.
Ojha, A., Sehitoglu, H., 2014. Twinning stress prediction in bcc metals and alloys. Philos. Mag. Lett. 94, 647–657.
Ojha, A., Sehitoglu, H., 2016a. Critical stress for the bcc–hcp martensite nucleation in Ti–6.25 at.% Ta and Ti–6.25 at.% Nb alloys. Comput. Mater. Sci. 111, 157–162.
Ojha, A., Sehitoglu, H., 2016b. Slip resistance of Ti based high temperature shape memory alloys. Shape Mem. Superelast. 2 (1), 50–61.
Ojha, A., Sehitoglu, H., 2016c. Critical stresses for twinning, slip, and transformation in Ti-based shape memory alloys. Shape Mem. Superelast. 2, 180–195.
Olson, G.B., Cohen, M., 1976a. A general mechanism of martensitic nucleation: part I. General concepts and the FCC→ HCP transformation. Metall. Trans. A 7, 1897–1904.
Olson, G.B., Cohen, M., 1976b. A general mechanism of martensitic nucleation: part II. FCC→ BCC and other martensitic transformations. Metall. Trans. A 7, 1905–1914.
Omori, T., Ando, K., Okano, M., Xu, X., Tanaka, Y., Ohnuma, I., Kainuma, R., Ishida, K., 2011. Superelastic effect in polycrystalline ferrous alloys. Science 333, 68–71.
Otsuka, K., Wayman, C.M., 1999. Shape Memory Materials. Cambridge university press.
Paranjape, H.M., Manchiraju, S., Anderson, P.M., 2015. A phase field-finite element approach to model the interaction between phase transformations and plasticity in shape memory alloys. Int. J. Plast. 80, 1–18.
Patoor, E., El Amrani, M., Eberhardt, A., Berveiller, M., 1995. Determination of the origin for the dissymmetry observed between tensile and compression tests on shape memory alloys. Le J. de Phys. IV 5. C2–495-C492-500.
Peierls, R., 1940. The size of a dislocation. Proc. Phys. Soc. 52, 34.
Porter, D.A., Easterling, K.E., Sherif, M., 2009. Phase Transformations in Metals and Alloys. CRC press (Revised Reprint).
Qidwai, M.A., Lagoudas, D.C., 2000. On thermomechanics and transformation surfaces of polycrystalline NiTi shape memory alloy material. Int. J. Plasticity 16, 1309–1343.
Richards, A.W., Lebensohn, R.A., Bhattacharya, K., 2013. Interplay of martensitic phase transformation and plastic slip in polycrystals. Acta Mater. 61, 4384–4397.
Saburi, T., Nenno, S., 1981. The shape memory effect and related phenomena. Solid Solid Phase Transform. 1455–1479.
Schoeck, G., 2011. The Peierls stress in a simple cubic lattice. Phys. Status Solidi B 248, 2284–2289.
Sedlak, P., Frost, M., Benešová, B., Zineb, T.B., Šittner, P., 2012. Thermomechanical model for NiTi-based shape memory alloys including R-phase and material anisotropy under multi-axial loadings. Int. J. Plasticity 39, 132–151.
Sehitoglu, H., Hamilton, R., Canadinc, D., Zhang, X.Y., Gall, K., Karaman, I., Chumlyakov, Y., Maier, H.J., 2003. Detwinning in NiTi alloys. Metall. Mater. Trans. A 34, 5–13.
Sehitoglu, H., Karaman, I., Anderson, R., Zhang, X., Gall, K., Maier, H.J., Chumlyakov, Y., 2000. Compressive response of NiTi single crystals. Acta Mater. 48, 3311–3326.
Sehitoglu, H., Karaman, I., Zhang, X.Y., Chumlyakov, Y., Maier, H.J., 2001. Deformation of FeNiCoTi shape memory single crystals. Scr. Mater. 44, 779–784.
Sehitoglu, H., Zhang, X.Y., Kotil, T., Canadinc, D., Chumlyakov, Y., Maier, H.J., 2002. Shape memory behavior of FeNiCoTi single and polycrystals. Metall. Mater. Trans. A 33, 3661–3672.
Simon, T., Kröger, A., Somsen, C., Dlouhy, A., Eggeler, G., 2010. On the multiplication of dislocations during martensitic transformations in NiTi shape memory alloys. Acta Mater. 58, 1850–1860.
Sinclair, C.W., Hoagland, R.G., 2008. A molecular dynamics study of the fcc→ bcc transformation at fault intersections. Acta Mater. 56, 4160–4171.
Sun, Q.-P., Xu, T.T., Zhang, X., 1999. On deformation of AM interface in single crystal shape memory alloys and some related issues. J. Eng. Mater. Technol. 121, 38–43.
Suzuki, H., 1962. Segregation of solute atoms to stacking faults. J. Phys. Soc. Jpn. 17, 322–325.
Thamburaja, P., Anand, L., 2001. Polycrystalline shape-memory materials: effect of crystallographic texture. J. Mech. Phys. Solids 49, 709–737.
Thamburaja, P., Anand, L., 2002. Superelastic behavior in tension–torsion of an initially-textured Ti–Ni shape-memory alloy. Int. J. Plasticity 18, 1607–1617.
Tseng, L.W., Ma, J., Hornbuckle, B.C., Karaman, I., Thompson, G.B., Luo, Z.P., Chumlyakov, Y.I., 2015a. The effect of precipitates on the superelastic response of [100] oriented FeMnAlNi single crystals under compression. Acta Mater. 97, 234–244.
Tseng, L.W., Ma, J., Wang, S.J., Karaman, I., Chumlyakov, Y.I., 2016. Effects of crystallographic orientation on the superelastic response of FeMnAlNi single crystals. Scr. Mater. 116, 147–151.
Tseng, L.W., Ma, J., Wang, S.J., Karaman, I., Kaya, M., Luo, Z.P., Chumlyakov, Y.I., 2015b. Superelastic response of a single crystalline FeMnAlNi shape memory alloy under tension and compression. Acta Mater. 89, 374–383.
Vollmer, M., Segel, C., Krooß, P., Günther, J., Tseng, L.W., Karaman, I., Weidner, A., Biermann, H., Niendorf, T., 2015. On the effect of gamma phase formation on the pseudoelastic performance of polycrystalline Fe–Mn–Al–Ni shape memory alloys. Scr. Mater. 108, 23–26.
Wang, J., Sehitoglu, H., 2013. Twinning stress in shape memory alloys: theory and experiments. Acta Mater. 61, 6790–6801.
Wayman, C.M., 1994. The phenomenological theory of martensite crystallography: interrelationships. Metall. Mater. Trans. A 25, 1787–1795.
Yang, X.-S., Sun, S., Wu, X.-L., Ma, E., Zhang, T.-Y., 2014. Dissecting the mechanism of martensitic transformation via atomic-scale observations. Sci. Rep. 4.
Yu, C., Kang, G., Kan, Q., 2014. Crystal plasticity based constitutive model of NiTi shape memory alloy considering different mechanisms of inelastic deformation. Int. J. Plasticity 54, 132–162.
Yu, C., Kang, G., Song, D., Kan, Q., 2015. Effect of martensite reorientation and reorientation-induced plasticity on multiaxial transformation ratchetting of super-elastic NiTi shape memory alloy: new consideration in constitutive model. Int. J. Plasticity 67, 69–101.
Zaki, W., Moumni, Z., 2007. A three-dimensional model of the thermomechanical behavior of shape memory alloys. J. Mech. Phys. Solids 55, 2455–2490.

Please cite this article in press as: Ojha, A., Sehitoglu, H., Transformation stress modeling in new Fe–Mn–Al–Ni shape memory alloy, International Journal of Plasticity (2016), http://dx.doi.org/10.1016/j.ijplas.2016.08.003